Harmonic analysis of climatological sea surface salinity

Tim P. Boyer and Sydney Levitus

Ocean Climate Laboratory/National Oceanographic Data Center, Silver Spring, Maryland, USA

[1]   A Fourier decomposition of the *World Ocean Atlas 1998* (WOA98) fields of climatological monthly mean salinity is used to describe the annual cycle of sea surface salinity (SSS). Global data sets of river runoff and evaporation minus precipitation (E−P) are used to put the annual cycle of SSS in the context of the global climate system. Most of the world ocean is shown to have an annual cycle of less than 0.3 on the practical salinity scale (PSS). Areas with an annual cycle larger than 0.3 include the northern Indian Ocean, the tropical Pacific and Atlantic, and the northern North Atlantic.   *INDEX TERMS:* 4504 Oceanography: Physical: Air/sea interactions (0312); 4532 Oceanography: Physical: General circulation; 4536 Oceanography: Physical: Hydrography; 4215 Oceanography: General: Climate and interannual variability (3309)

1.   Introduction

[2]   Due to the lack of quality salinity measurements on the same temporal and spatial scale as temperature measurements, many studies of the ocean's role in the Earth's climate system rely on temperature measurements alone. However, as a parameter of state, salinity along with temperature and pressure, determine the density of seawater which determines ocean currents. There is recognition that salinity must be taken into consideration. The Climate Variability and Predictability World Climate Research Program (CLIVAR) implementation plan [*CLIVAR*, 1998] states that surface and subsurface salinity are important to understanding and predicting climate variability. Knowledge of salinity variability is important for interpretation of dynamic height measured from altimetric data in areas where the halosteric component of sea level is comparable and opposite in sign to the thermosteric component [*Antonov et al.*, 2002; *Lukas*, 2001; *Maes*, 1998; *Levitus*, 1989]. Furthermore, salinity plays a large role in the formation of the barrier layer in the western tropical Pacific [*Lukas and Lindstrom*, 1991; *Vialard and Delecluse*, 1998], and thus may play a role in El Niño generation [*Henin et al.*, 1998]. A barrier layer in the western Atlantic is associated, in part, with vertical salinity variations originating in the Amazon River [*Pailler et al.*, 1999]. Salinity variation is important to the circulation in regions of the Indian Ocean [*Shenoi et al.*, 1999; *Kumar and Prasad*, 1999; *Beal et al.*, 2000]. Events such as the Great Salinity Anomalies in the North Atlantic [*Dickson et al.*, 1988; *Belkin et al.*, 1998] provide a salinity signature of ocean variability at periods greater than 1 year. In some areas of the ocean, such as the California Current System [*Batteen et al.*, 1995] and the Leeuwin Current System [*Batteen and Huang*, 1998], salinity and temperature are both necessary to adequately characterize the large scale circulations.

[3]   Sea surface salinity (SSS) is singularly important in understanding salinity variability, as the oceans surface is in direct contact with atmospheric forcing, such as evaporation, precipitation, and winds. SSS is also directly affected by river runoff and ice melt/formation. SSS is used as a boundary condition for general circulation models forced by the changing fresh water flux on the surface [*Barnier et al.*, 1995].

[4]   The purpose of the present study is to present a quantitative description of SSS on a global scale using Fourier decomposition of monthly means of in situ SSS data from objectively analyzed hydrographic data. The recent release of the *World Ocean Database 1998* (WOD98) has made available additional modern and historical salinity measurements from bottles and CTDs which greatly expand the temporal and spatial distribution of these measurements over previously available data sets [*Boyer et al.*, 1998a, 1998b; *Levitus et al.*, 1998]. In addition, the ORSTROM group of New Caledonia has greatly increased the number of surface bucket and thermosalinograph measurements in the tropical Pacific as part of the SURTROPAC (Survey of the Tropical Pacific) program [*Henin and Grelet*, 1996]. Bucket measurements from this program through 1991 are included in the WOD98.

[5]   Previous studies of SSS have been confined to specific regions of the world ocean: *Smed* [1943] for the North Atlantic, *Taylor* [1980] for Atlantic weather stations, *Taylor* [1983] for the northeast Atlantic, *Dessier and Donguy* [1994] for the tropical Atlantic, *Donguy* [1994], *Delcroix et al.* [1996], and *Delcroix* [1998] for the tropical Pacific, and *Donguy and Meyers* [1996a] for the tropical Indian Ocean. A previous study of the climatological annual cycle of SSS on a global scale [*Levitus*, 1986] was limited, through lack of data, to inspection of differences by seasons. The advantage of the global approach is in being able to compare and contrast the annual cycle in different regions

of the worlds ocean. This provides the basis for understanding of where the annual cycle is of a scale which makes it important to the global climate system. It also facilitates comparison of the SSS annual cycle to other parameters involved in the global climate annual cycle. To illustrate this last point, the climatological annual cycle of two parameters related to the world's fresh water balance, evaporation minus precipitation (E−P) and river-runoff will be compared to the SSS fields. A global comparison of the Fourier components of SSS with the same E−P Fourier components (monthly mean E−P climatological monthly fields estimated from ship weather reports [*da Silva et al.*, 1994]) may help to reveal comparable large scale patterns in the two fields. Complicating a quantitative comparison is the problem of the lack of reliable historical precipitation measurements and inaccuracies in estimates of evaporation. Hence, our purpose here is to simply identify regions where large-scale patterns in SSS variability may be caused by similar large-scale variability in E−P fields.

2.   Data and Method

2.1.   Salinity Data

[6]   The salinity fields for this study are the objectively analyzed gridded monthly salinity climatologies from the *World Ocean Atlas 1998* (WOA98) series [*Boyer et al.*, 1998c, 1998d, 1998e]. WOA98 consists of climatologies of oceanographic variables created from the profile data assembled in the WOD98 database. The objective analysis technique is described in detail in the given references, so only a brief overview is given here. All data which passed quality control procedures [*Boyer and Levitus*, 1994] is binned into means over one-degree latitude-longitude grid-boxes. The mean is taken to represent the value at the center of each grid-box. Climatological means are then calculated by taking a distance weighted average of the mean value in all grid-boxes with data within a given radius of influence around the center of a given grid-box minus a first-guess field. This value is then added to the mean at the center of the grid-box. This process is repeated three times with successively smaller radii of influence: 880, 660, 440 km. The first-guess field for the annual mean is a zonal average. The first-guess for each season is the annual climatological field, and the first-guess for each monthly field is the appropriate seasonal climatology. The WOA98 monthly analyzed fields were modified by reinserting the observed one-degree square monthly means into the corresponding objectively analyzed monthly mean temperature and salinity field. Then new monthly mean gridded fields were computed using the annual mean and first two harmonics from the Fourier analysis [*Bloomfield*, 1976]. One median smoother of radius one-degree in latitude and longitude was then performed. Finally, the resulting temperature and salinity fields were stabilized with respect to the Hessel-burg-Sverdrup stability criteria [*Lynn and Reid*, 1968] calculated from the two fields. These modifications were performed to sharpen the gradients in high gradient areas, such as the Gulf Stream, among other considerations.

[7]   The database used as input of the climatologies, WOD98, contains all profile data archived at the U.S. National Oceanographic Data Center in Silver Spring, Maryland and the colocated World Ocean Data Center for Ocean-

ography as of 1994, as well as all profile data collected as part of the IOC (Intergovernmental Oceanographic Commission) Global Ocean Data Archeology and Rescue (GODAR) project. Also included are bucket salinity measurement in the tropical Pacific, from the SURTROPAC program. The total number of SSS observations exceeds 1.4 million.

[8]   The WOD98 SSS data show a wide variability of distribution, both spatially and temporally. There is consistently more data for the northern hemisphere than the southern. In each hemisphere, the amount of data from the respective winter months is less than for the respective summer hemisphere. Data is sparse in all years until the mid-1950s. To provide information of the representativeness of a Fourier decomposition of SSS for different geographic regions, Figure 1 shows the number of months of data within the first radius of influence (880 km) of the objective analysis for each one-degree longitude-latitude grid box. Data are sparse in the central ocean basins of the southern hemisphere and most of the Southern Ocean.

[9]   The annual mean and the standard deviation of the monthly mean WOA98 climatological fields about the annual mean are shown in Figures 2a and 2b. The amplitude, phase, and percent variance accounted for by the first harmonic of SSS are shown in Figures 3a–3c, respectively. For the second harmonic the amplitude and percent variance accounted for are presented in Figures 4a and 4b. All values for salinity are from the practical salinity scale (PSS) and are unitless. The phase of the second harmonic is not shown due to its relative unimportance over most of the world ocean.

2.2.   E−P Data

[10]   The E−P fields presented are the annual mean, standard deviation of the monthly means about the annual mean, and the amplitude and phase of the first harmonic of the monthly mean climatologies of *da Silva et al.* [1994]. These E−P fields were calculated from estimates of evaporation and precipitation based on the "present weather" code from historical ship weather records. Hence these are crude estimates that we use qualitatively. The annual mean of the 12 monthly climatologies for E−P is shown in Figure 5a and the standard deviation of the monthly mean fields about the annual mean field is shown in Figure 5b. Figure 6a presents the amplitude of the first harmonic. Figure 6b shows the phase of the first harmonic, representing the annual maximum of E−P. The units for all E−P fields are mm/day. The original units used by da Silva et al. were mm/3 hours (corresponding to the interval between ships weather reports).

2.3.   River Runoff Data

[11]   The Global Runoff Data Center (GRDC) in Koblenz, Germany archives river gauge data measurements of river flow volumes from rivers around the world. Not every river is gauged, and many important sources of riverine input are not measured by this means. There are numerous small-length rivers in the Indo-Pacific archipelago which channel large amounts of fresh water to the ocean for which the GRDC has no information. *Forsbergh* [1969] estimates that the small rivers that empty into the Gulf of Panama cumulatively add as much fresh water to the ocean as 64% of the outflow of the Mississippi River. Examination of the mean monthly outflows from major, gauged rivers [*Balázs et al.*, 2000] in comparison to the annual cycle of
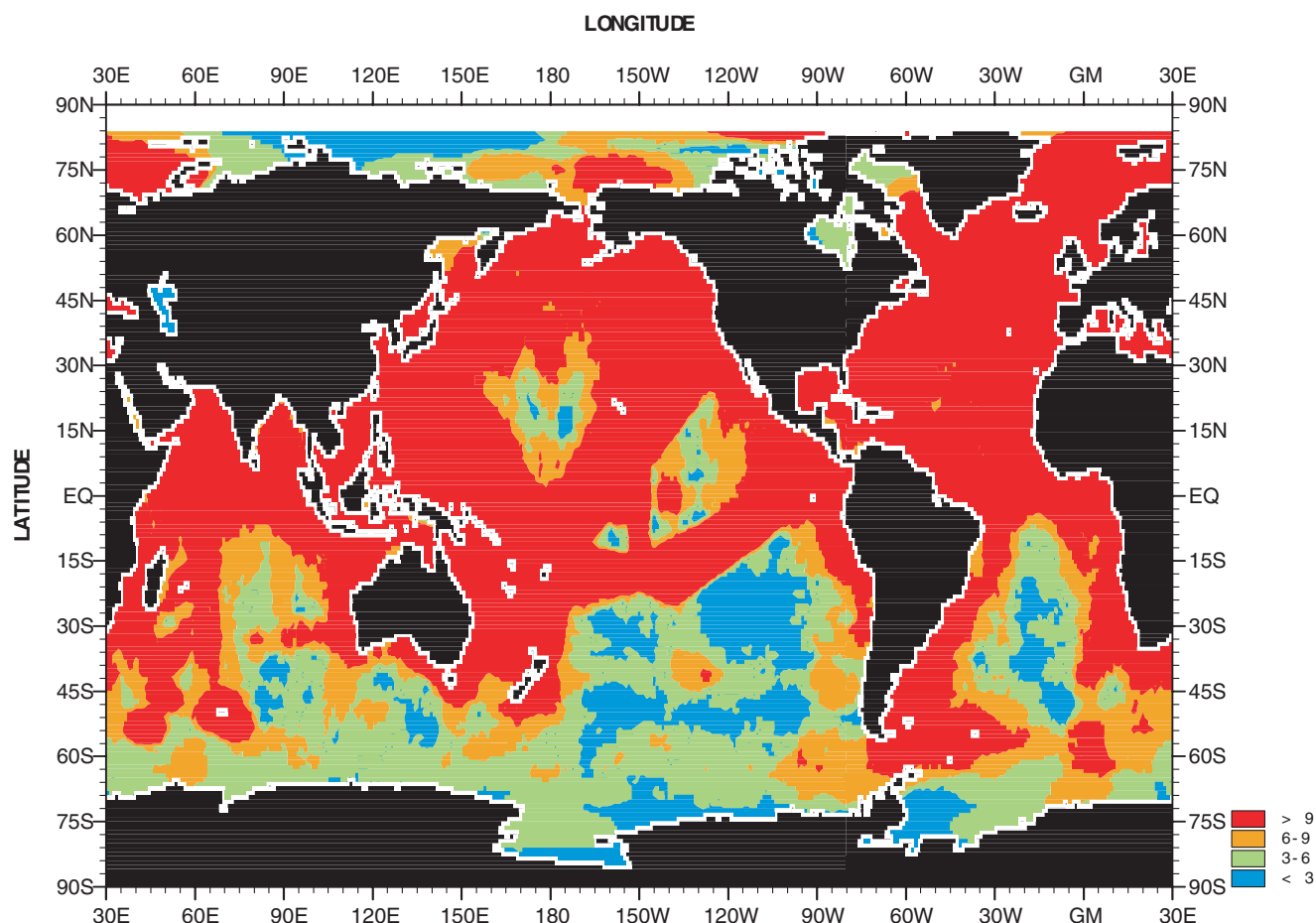
Figure 1.   Number of months contributing data within the influence region surrounding each one-degree square from WOD98.

SSS reveal the relative importance of the riverine input to the SSS of the area within 300 km of the rivers' mouths.

[12]   Table 1 shows statistics for some of the highest flow volume rivers in the world. The important riverine input variables for the annual cycle of SSS in the ocean are the annual range of outflow volume and the month of minimum outflow. The former is an important consideration, since, while fresh water outflow may affect local and remote salinity, the annual cycle of salinity may not be much affected by freshwater input if that input does not change much over the course of the year. However, seasonal variability in ocean circulation may redistribute the riverine output. For instance, the St. Lawrence River has an effect on the SSS of the Labrador Sea and coastal U.S. waters [*Khatiwala et al.*, 1999], but the annual range of outflow volume is relatively small, as the monthly mean outflow changes little throughout the entire year. As a result, the annual range of outflow volume of the St. Lawrence River, by itself, has little effect on the annual cycle of SSS. Changes in the advection pattern in the affected areas, which carry the St. Lawrence River outflow, are the important factor.

2.4.   Sources of Error

[13]   Several sources of error contribute to uncertainties in the results presented here. Lack of data is most probably the largest source of error. As we have shown, salinity data are relatively sparse. It is possible to quantify this error only by addition of more data, modern as well as historical. Our work should be viewed as a best estimate that can be made with presently available data. As additional data become available our analyses will be updated.

[14]   Salinity measurement errors of $0.02-0.03$ are typical of the titration technique used to make many of the salinity measurements contained in WOD98. Salinometers and modern CTD instruments measure salinity to an accuracy on the order of 0.005 PSS. The relatively large errors associated with bucket measurements from the SURTRO-PAC program, between 0.1 and 0.2 [*Henin and Grelet*, 1996] are offset by their large numbers. More than 46% of the SSS data in the tropical Pacific from WOD98 comes from this bucket data, and the geographical coverage in the tropical Pacific would be inadequate without its inclusion. *Reverdin et al.* [1994] discuss other sources of measurement and recording errors in SSS data. The standard error of the mean for SSS from WOD98 data is less than 0.1 over most of the world ocean, with values between 0.1 and 0.2 in scattered areas, concentrated mostly near-coasts.

[15]   We have computed the root-mean square-deviation (RMSD) between the monthly mean salinity fields of WOA98 and the monthly mean fields reconstructed from the annual mean and the first two harmonics (not shown).
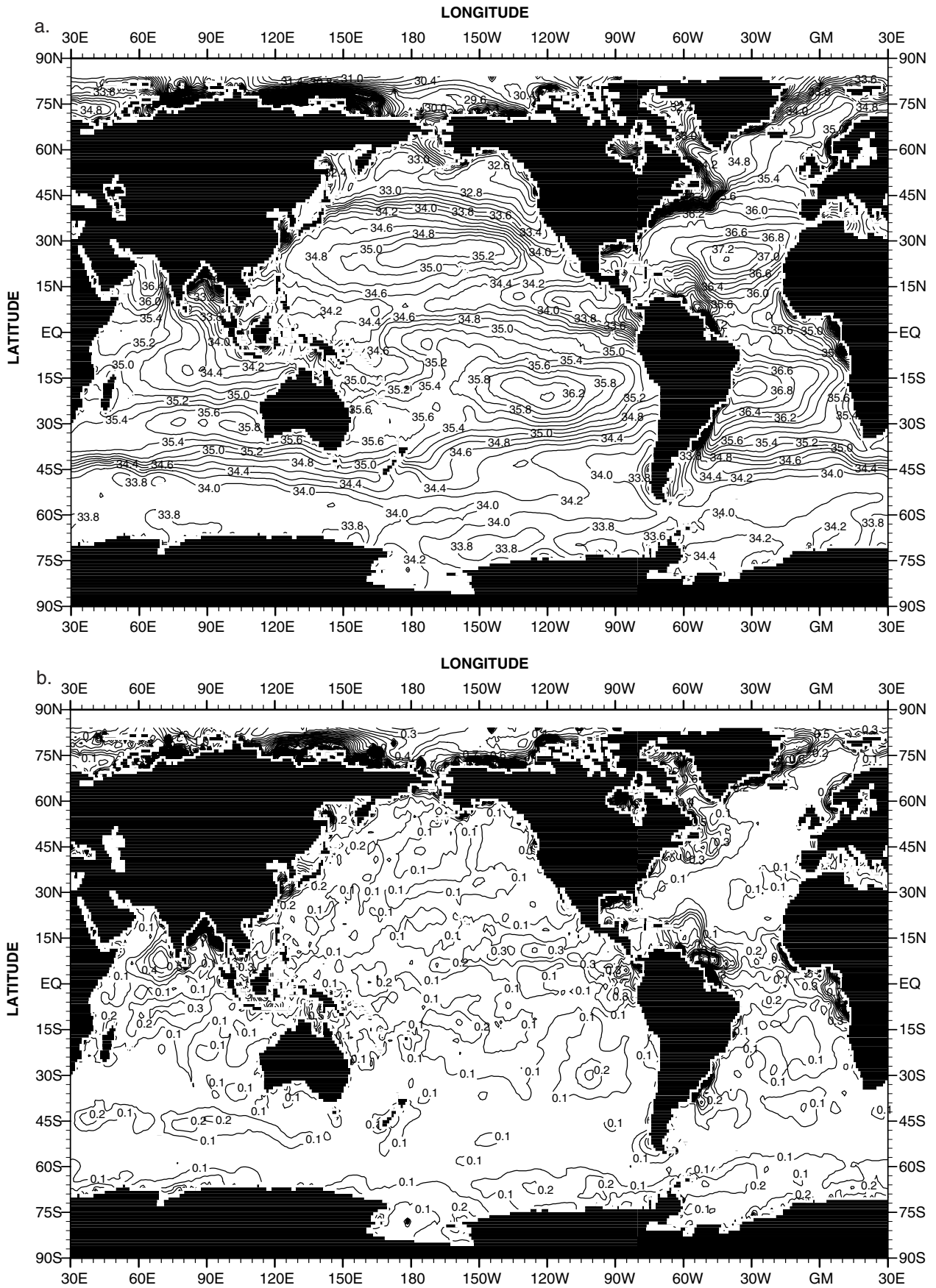
Figure 2. (a) Annual mean SSS from WOA98. (b) Standard deviation of the monthly mean SSS fields about the annual mean.
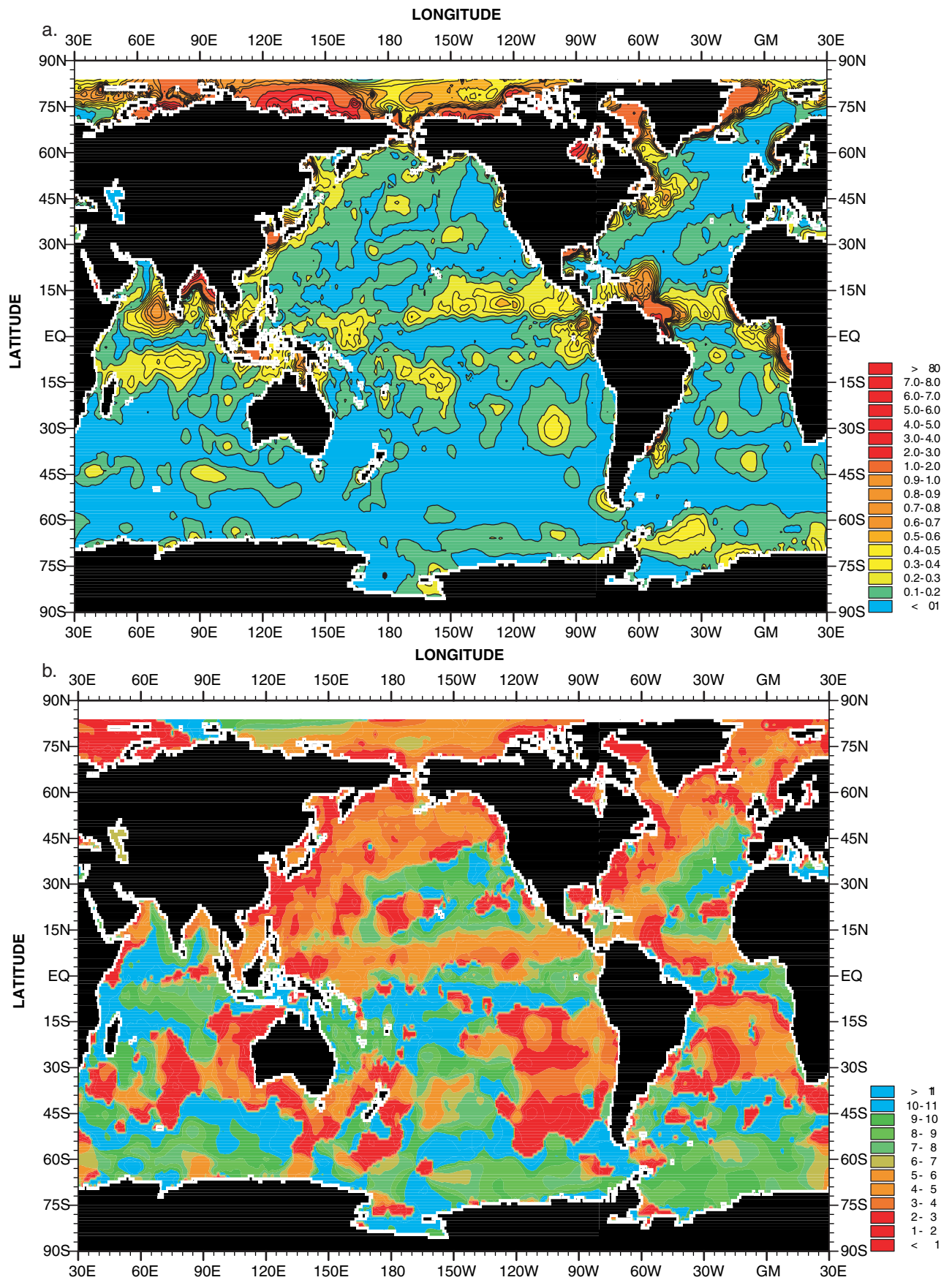
Figure 3. (a) Amplitude of the first harmonic of SSS. (b) Phase (month of maximum SSS) of first harmonic. (c) Percent of total variance accounted for by the first harmonic of SSS.
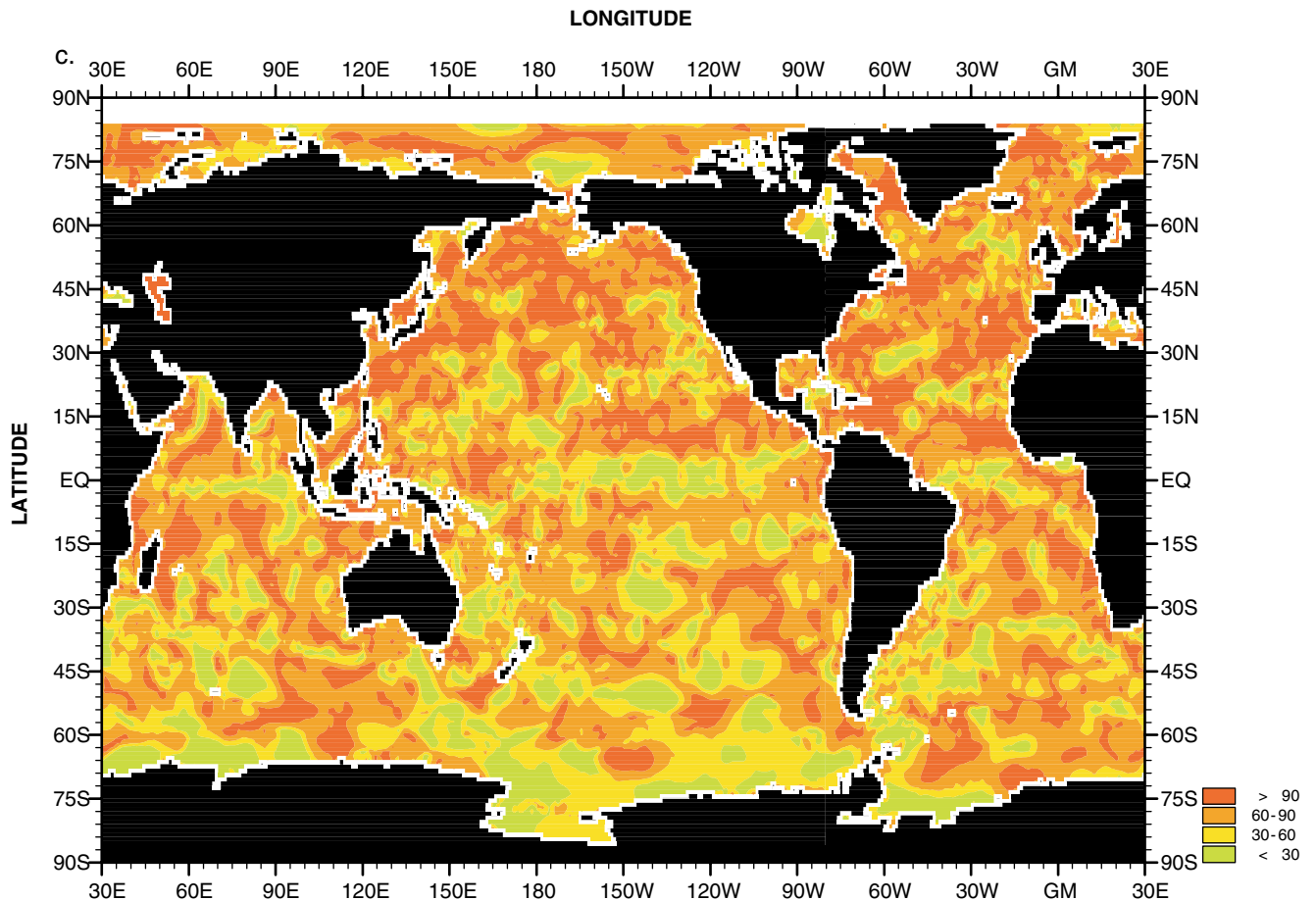
Figure 3. (continued)

The RMSD is less than 10% of the total variance for most of the world ocean, with areas between 10% and 25% in the northeast North Pacific, western tropical Pacific, and central basins of the southern hemisphere.

[16] It is possible in principal to compute the uncertainty associated with the Fourier coefficients [*Taylor*, 1997] that we have computed at each grid point. This requires knowledge of the standard deviation of SSS at each grid point and use of the Law of the Propagation of Errors. However, there are not many data for each month at most grid points. Therefore, we simply do not have good estimates of the RMSD of salinity in each grid point for each month and thus do not have enough data to compute the variance or standard deviation of the amplitude and phase just based on the data in each individual 1-degree gridbox. Our objective analysis procedure uses data from surrounding grid points (that is all data within an ''influence region'') about each grid point to produce a ''correction'' to a ''first-guess'' value at each grid point being analyzed. In this way we increase statistical significance but at the expense of not being able to resolve small-scale features that may exist in the actual data field. This is a reasonable trade-off since the smallest Fourier component that can be represented has a wavelength of about 6–8 times the grid point spacing [*Levitus*, 1982]. What is required for a proper estimate of interpolation error of our computed analyzed grid point estimates is to compute the error covariances within the influence region. However,

with sparse data such as SSS, this is difficult. Optimal interpolation methods are supposed to use error covariances computed from climatological data. In our case (SSS) we are creating ''climatologies'' but barely have enough data to define the mean in many places much less a higher order statistic such as a covariance function. For this reason we believe that Figure 1 in this paper is as meaningful as any type of error analysis that can be produced.

[17] For the E−P fields, measurement and recording errors are discussed, but not quantified, by *da Silva et al.* [1994]. No estimates of error associated with the calculation of the objectively analyzed fields are provided. The RMSD error for the Fourier decomposition show larger proportion of variance than for SSS. Most of the North Pacific, North Atlantic, and North Indian Oceans have RMSD error <25% of total variance, but there are significant areas with RMSD errors between 25% and 50% of total variance. Directly along the equator in the Pacific and Atlantic, RMSD errors reach 100% of total variance. South of 30°S, most of the ocean has RMSD errors of around 100%.
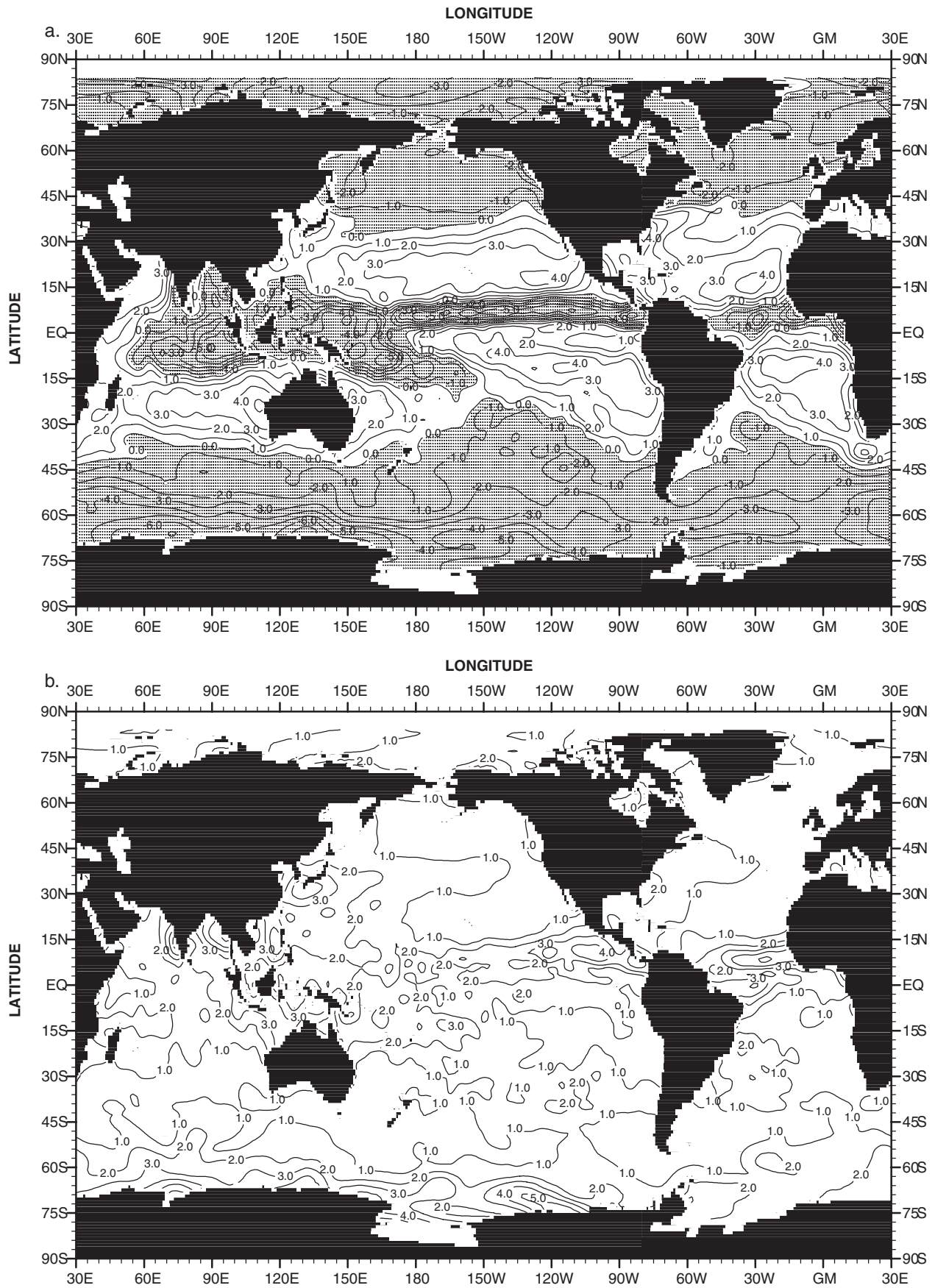
3.   Results

3.1.   Annual Cycle of SSS

[18] Figure 3a shows that large portions of the world ocean have an annual cycle of SSS less than 0.2, with much of these areas having annual amplitude of SSS less than 0.1.
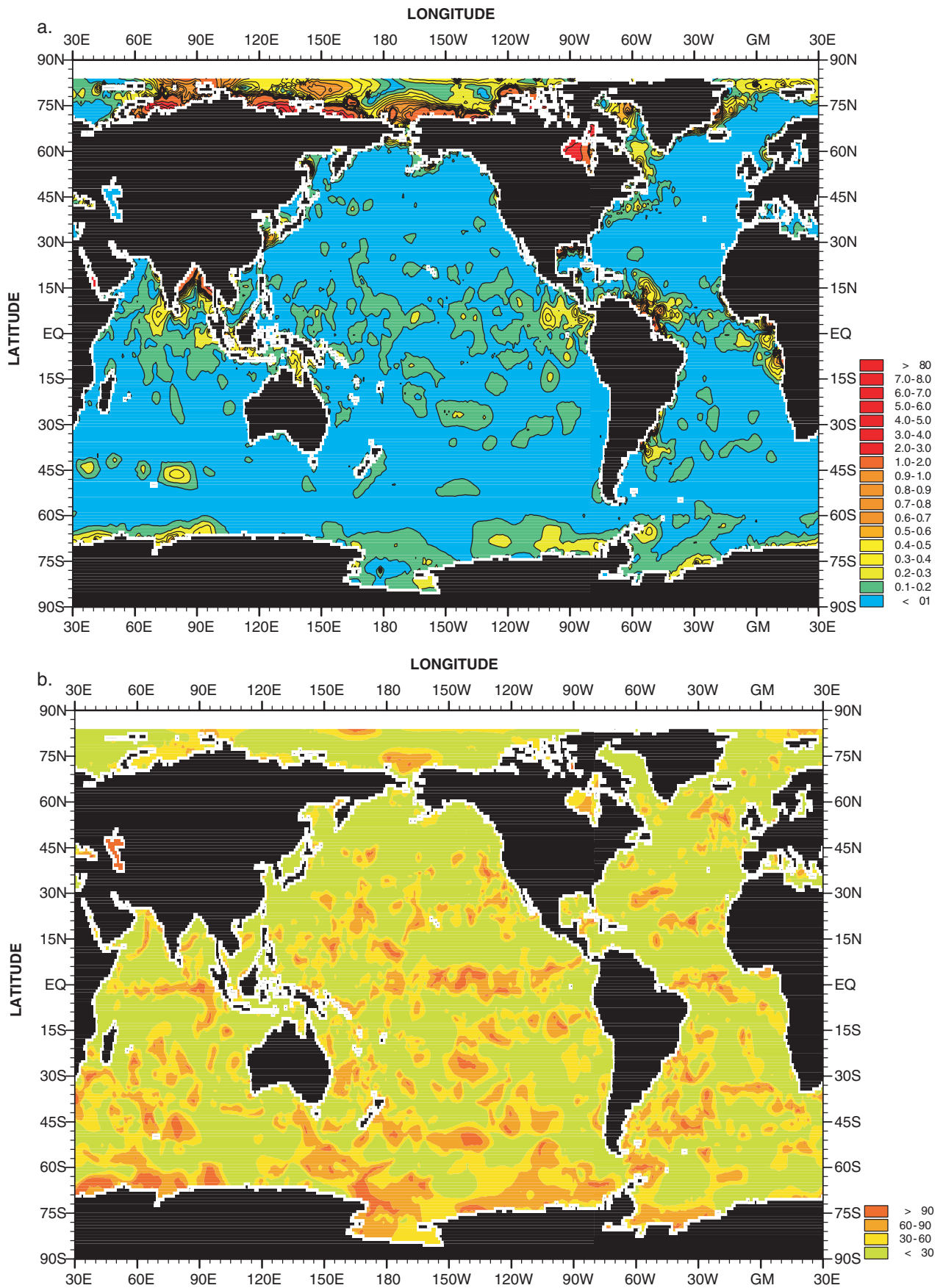
Figure 4. (a) Amplitude of the second harmonic of SSS. (b) Percent of total variance accounted for by the second harmonic of SSS.

Figure 5.   (a) Annual mean E−P (mm/day) (stippling denotes negative values). (b) Standard deviation (mm/day) of the monthly mean E−P fields about the annual mean.
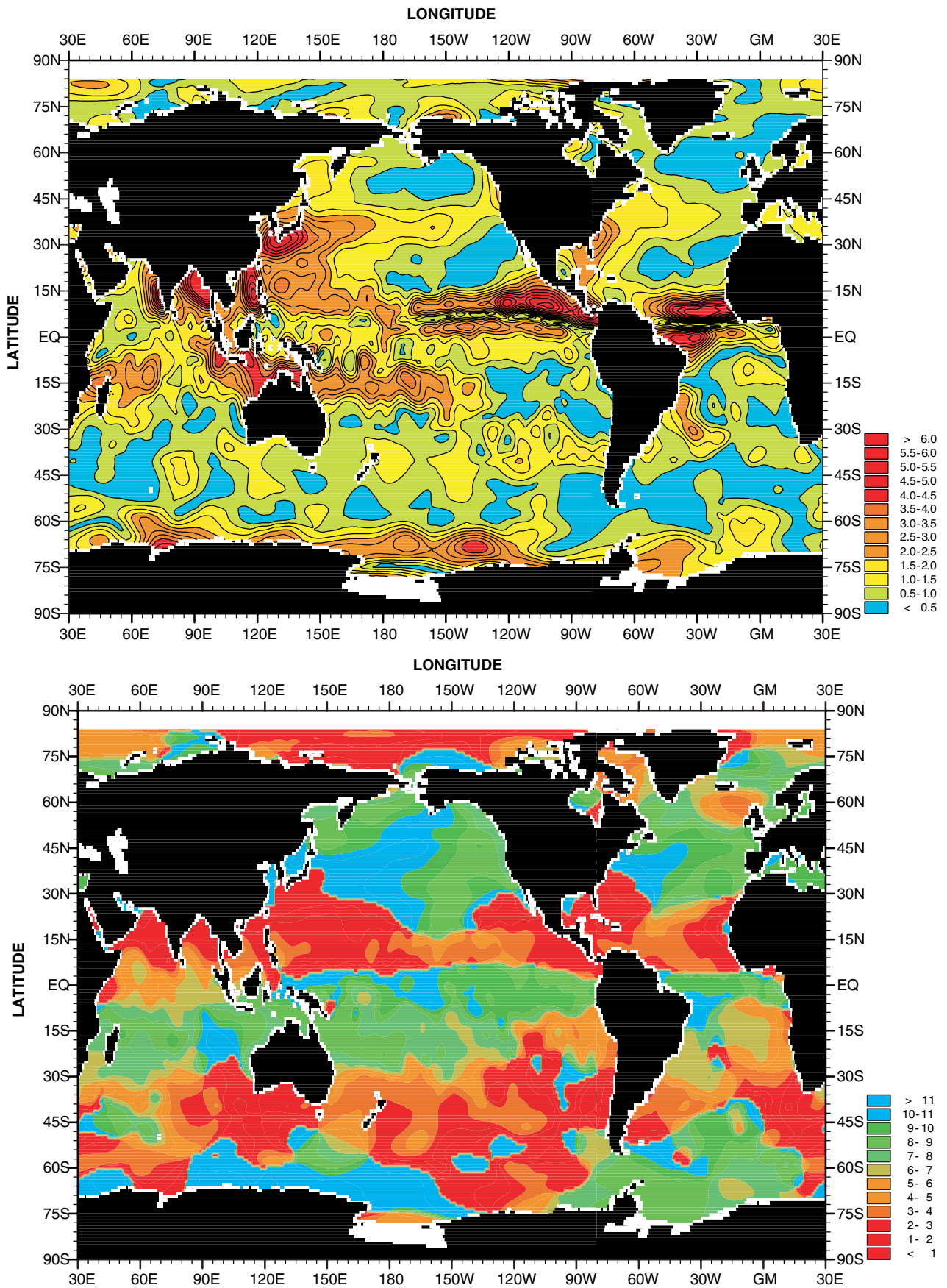
Figure 6. (a) Amplitude (mm/day) of the first harmonic of E−P. (b) Phase (months) of the first harmonic of E−P.

Table 1. Comparison of River Outflow With Amplitude and Phase of Salinity First Harmonic Within 300 km of River Mouths[a]

River	Outflow Volume Annual Range, m^3/s	Minimum Outflow Month (volume, m^3/s)	SSS Amplitude	SSS Phase
Amazon	130,000	November (110,000)	1.0–10.0	November–January
Orinoco	58,000	March (7,110)	0.6–4.5	February–April
Ganges	42,000	April (1,751)	1.0–8.0	March–April
Brahmaputra	40,000	February (4,160)	1.0–8.0	March–April
Yangzte	38,000	January (10,099)	0.3–1.6	January–February
Congo	24,000	August (31,086)	1.3–2.0	July–August
Mississippi	19,000	September (9,579)	0.5–2.0	October–January

[a]River outflow data from University of New Hampshire/Global Runoff Data Center (Koblenz, Germany).

Areas with a SSS annual cycle greater 0.3 include the tropical Pacific and Atlantic, the Indo-Pacific throughput area, much of the North Indian, areas with seasonal ice cover, the area between China and Japan, the eastern Caribbean, and parts of the South Atlantic near the African and South American coasts. The following sections examine specific areas in more detail.

3.1.1. North Atlantic

[19] One of the first works describing the annual cycle of SSS was by *Smed* [1943], hereafter referred to as SM43. His work shows the amplitude and phase of the first harmonic of SSS for the North Atlantic (Figures 13–14, respectively, in SM43, reproduced as Figures 9–10 by *Levitus* [1986]). Comparison of the present results and SM43 document that the basic features in both analyses are quite similar outside the tropics. *Reverdin et al.* [1994] state that SM43 should not be used south of 50°N due to uncertainties in the quality of the data. However, the Fourier decomposition of SM43 matches quite well with our present results (which are based on a completely different data set) north of 25°N, south of which SM43 discusses uncertainties in the fields. Outside the tropics, both studies show a relatively low amplitude tongue extending from between Iceland and the British Isles southwest to the eastern Caribbean. To the southeast and northwest of this tongue, amplitudes of 0.1 to 0.2 are found, which extend to the coast near the Mediterranean Sea in the present study, though not in SM43. The phase of the first harmonic for SSS shows similar patterns in both studies. The area of the North Atlantic to the northwest of a line running southwest from Great Britain to the Caribbean is characterized by salinity maxima occurring between February and April. On the southeast side of the line, the salinity maximum occurs later in the year, August through November.

[20] The large change of sea-ice coverage, representing brine rejection during formation and release of fresh water during melting, has a direct effect on SSS in much of the northern North Atlantic. The phase of the first harmonic for SSS for most northern Atlantic areas which are ice-covered for only part of the year, including Baffin Bay, the Labrador Sea, and the Greenland Sea, is centered on March (Figure 3b). This is the month of maximum ice coverage for these areas [*Parkinson et al.*, 1999]. The amplitude of the first harmonic of SSS in areas of ice cover in the northern North Atlantic is quite large, generally greater than 1.0 in Baffin Bay, east of Greenland, and in the western Labrador Sea. The cycle of salinity in partially ice-covered areas, such as the Labrador Sea, is augmented by the advection of water from other ice-covered areas, such as Baffin Bay, and the

area east of Greenland, via the Greenland Current [*Khatiwala et al.*, 1999].

3.1.2. The Tropical Atlantic, Amazon Outflow, and Caribbean

[21] The western tropical Atlantic SSS cycle is dominated by the outflow of Amazon River water, which enters the ocean near the equator. The Amazon is the river with the largest annual range in outflow volume in the world. The maximum outflow for the river is more than 240,000 m^3/s and occurs in July. The minimum mean monthly outflow is slightly more than 110,000 m^3/s and occurs in November [*Balázs et al.*, 2000]. The month of maximum salinity within 300 km of the river mouth varies from November to January (Table 1), in agreement with the period of minimum outflow. The largest extent of the plume, as designated by a salinity of less than 34.0, is not in July, but earlier, between March and May. This is due to the prevailing winds in the area [*Lentz*, 1995]. The effects of the river outflow are seen far from this plume. The amplitude of the first harmonic is about 1.0 at 12°N, and larger than 0.2 as far north as 24°N (Figure 3a). The effects extend all the way into the eastern Caribbean, where the amplitude is greater than 0.2. This is partly the result of entrainment of Amazon discharge in the southwestward flowing Guiana Current [*Borstad*, 1982]. The effects have been noted as far north in the Caribbean as coastal Puerto Rico [*Froelich et al.*, 1978]. Froehlich et al. do not differentiate between the waters of the Orinoco River and the Amazon. The Orinoco River, which drains into the Atlantic northwest of the Amazon, near 9°N, also has a very large annual range in volume output (Table 1). Most of the Orinoco waters travel north-northwest into the eastern Caribbean [*Bonilla et al.*, 1993], suggesting that the influence of the Orinoco in the eastern Caribbean may be more important than that of the Amazon [*Müller-Karger et al.*, 1989]. Furthermore, although the central and eastern tropical Atlantic surface salinity field is dominated by E−P variations [*Dessier and Donguy*, 1994, hereafter referred to as DD94] related to rainfall under the seasonally migrating ITCZ, as much as 70% of Amazon Plume water is carried eastward across the Atlantic in the Northern Brazil Current retroflection from August to October [*Lentz*, 1995].

[22] DD94 present the amplitude of the first harmonic of SSS in the tropical Atlantic almost exclusively from bucket measurements. Their results generally agree with the results of the present study. One exception is the high amplitude area off the west coast of Africa centered at 10°N, which is confined to the coast in the present study, but which extends nearly to 20°W as shown by DD94. The phase of the first

harmonic for the two studies is also similar (note that DD94 shows the month when the SSS minimum occurs).

[23] Other areas of SSS greater than 0.3 annual amplitude in the Atlantic Ocean include the northern Gulf of Mexico and the west coast of Africa below the equator. This later is associated, in part, with the outflow of the Congo River. The month of minimum outflow for the Congo immediately precedes the phase of the first harmonic of salinity in the area near the river mouth (Table 1). In the northern Gulf of Mexico, the Mississippi River's cycle of outflow appears to be only one factor in the determination of the first harmonic of SSS. Minimum outflow occurs in September, but the maximum salinities in the area are not reached until December–January.

3.1.3. Pacific Ocean

[24] Most of the North Pacific outside of the tropics exhibits an SSS amplitude less than 0.3. The tropical Pacific has a coherent band of SSS amplitude greater than 0.3 north of the equator, decreasing to between 0.2 and 0.3 west of the dateline (Figure 3a). Much of the study of SSS in the world ocean has been concentrated in the tropical Pacific, due to interest in El Niño events. Interannual variability in this area is at least as important as the annual cycle in general [*Cane*, 1982]. For SSS, *Delcroix et al.* [1996] estimated, using EOF analysis of bucket and thermosalinograph data, that only 17% of the total variability in the tropical Pacific west of 140°W can be attributed to the annual cycle. However, Figure 3a shows there is still a substantial annual cycle in this area. Much of the variability is due to rainfall related to the position of the Intertropical Convergence Zone (ITCZ). The area of relatively large salinity amplitude associated with the changing position of the ITCZ (as defined by *Waliser and Gautier* [1993]), runs roughly from as far north as 15°N off the coast of Mexico, westward to very near the equator near the island of New Guinea (Figure 3a). The amplitude of the first harmonic is greater than 0.2 over most of this area, exceeding 0.5 near 120°W. The eastward flowing North Equatorial Counter Current (NECC) has a large annual transport volume cycle [*Donguy and Meyers*, 1996b] peaking in northern winter. It transports lower salinity western Pacific water eastward, adding to the salinity variability in this area. The South Pacific Convergence Zone (SPCZ) extends southeast from the edge of the ITCZ near New Guinea into the central southern Pacific. Seasonal changes in the extent of the SPCZ and the attendant cycle in precipitation account for some change in the amplitude of the annual SSS cycle in this region [*Alory and Delcroix*, 1999]. This change in the amplitude of the annual SSS cycle is evident in Figure 3a, although it is not coherent.

[25] The Indo-Pacific archipelago encompasses areas of high annual SSS variability. The area of the Lombok Straits, one of the most important exchange points between Indian and Pacific waters, has an annual cycle >0.5 (Figure 3a). Advection in this area is closely linked to the monsoon cycle, and has a large semiannual component [*Yamagata et al.*, 1996]. This area is also subject to seasonal input from a number of small rivers [*Miyama et al.*, 1996]. Likewise, there is large amplitude in the annual cycle of E−P (Figure 6a) over the southern Indo-Pacific archipelago which accounts for some of the variability found in the SSS field.

[26] The amplitude of the first harmonic of E−P in the tropical Pacific is relatively large compared to surrounding areas. There is a local maxima near 120°W in the tropical Pacific corresponding to a similar maximum in the amplitude of the first harmonic of SSS. Like the SSS field, the amplitude of the annual cycle of E−P is more pronounced to the east in the tropical Pacific. The feature which corresponds to the SPCZ is more zonal in the E−P field than in the SSS field. In the southwest North Pacific is an area of high E−P variability which, in noncoastal areas, does not have a counterpart in the SSS field. However, near the coast, there is a large amplitude in the first harmonic of SSS. Other factors aside from E−P also contribute here, including the on-shelf movement of the Kuroshio and the Yangtze River outflow [*Hur et al.*, 1999]. The Yangtze also has a significant and direct effect on the surrounding ocean. Its month of minimum outflow is January (Table 1), and the maximum salinity in the area is found in January and February.

[27] *Delcroix* [1998] has estimated that the SSS minimum lagging behind the maximum in precipitation by 2–3 months in the region of the ITCZ in the Pacific. In our results in this same region, we see the phase of the first harmonic of SSS lags behind the phase of the first harmonic of E−P by 1–3 months. A phase lag of 3 months between precipitation and SSS would be expected if precipitation were the dominant source of SSS variability in the annual period [*Hires and Montgomery* 1972; *Delcroix et al.*, 1996]. In comparing the Fourier decompositions of SSS and E−P, much of the relationship between the two can be obscured by other factors, such as advection and/or mixing. However, a comparison of the phases of the two fields on a global scale can reveal where E−P may be the dominant factor in the SSS annual cycle. Figure 7 shows the phase lag between the annual cycle of SSS and the annual cycle of E−P. Following *Delcroix et al.* [1996], areas where the phase lag is positive and from 1–3 months may be dominated by E−P changes. The areas under the ITCZ in the Pacific, north of the equator, and in the Indian, south of the equator exhibit this relationship, although the relationship in the western Pacific is relatively weaker. The Atlantic areas under the influence of the ITCZ exhibit this relationship near the equator, but the phase lag is greater than 3 months further north. In the area influenced by the SPCZ, the phase lag is from 0 to 3 months, with some areas greater than 3 months, and small areas with a negative phase lag.

3.1.4. Indian Ocean

[28] The regime in the northern Indian Ocean is influenced by circulation and E−P patterns associated with the monsoon cycle and by river input. The two basins separated by the Indian subcontinent are the Arabian Sea, characterized by relatively high salinity water, and the Bay of Bengal, characterized by relatively low salinity water (Figure 2a). The amplitude of the first harmonic shows two significant features. The first feature is centered along 9°S, coincident with the position of the ITCZ [*Waliser and Gautier*, 1993] during part of the year (Figure 3a). An area of relative maxima in the E−P annual cycle is also evident in this area. The second is a region centered at 8°N, 70°E termed the Laccadive High that was first identified by *Bruce et al.* [1994] on the basis of hydrographic and altimeter data. A maximum in the amplitude of the first harmonic of E−P
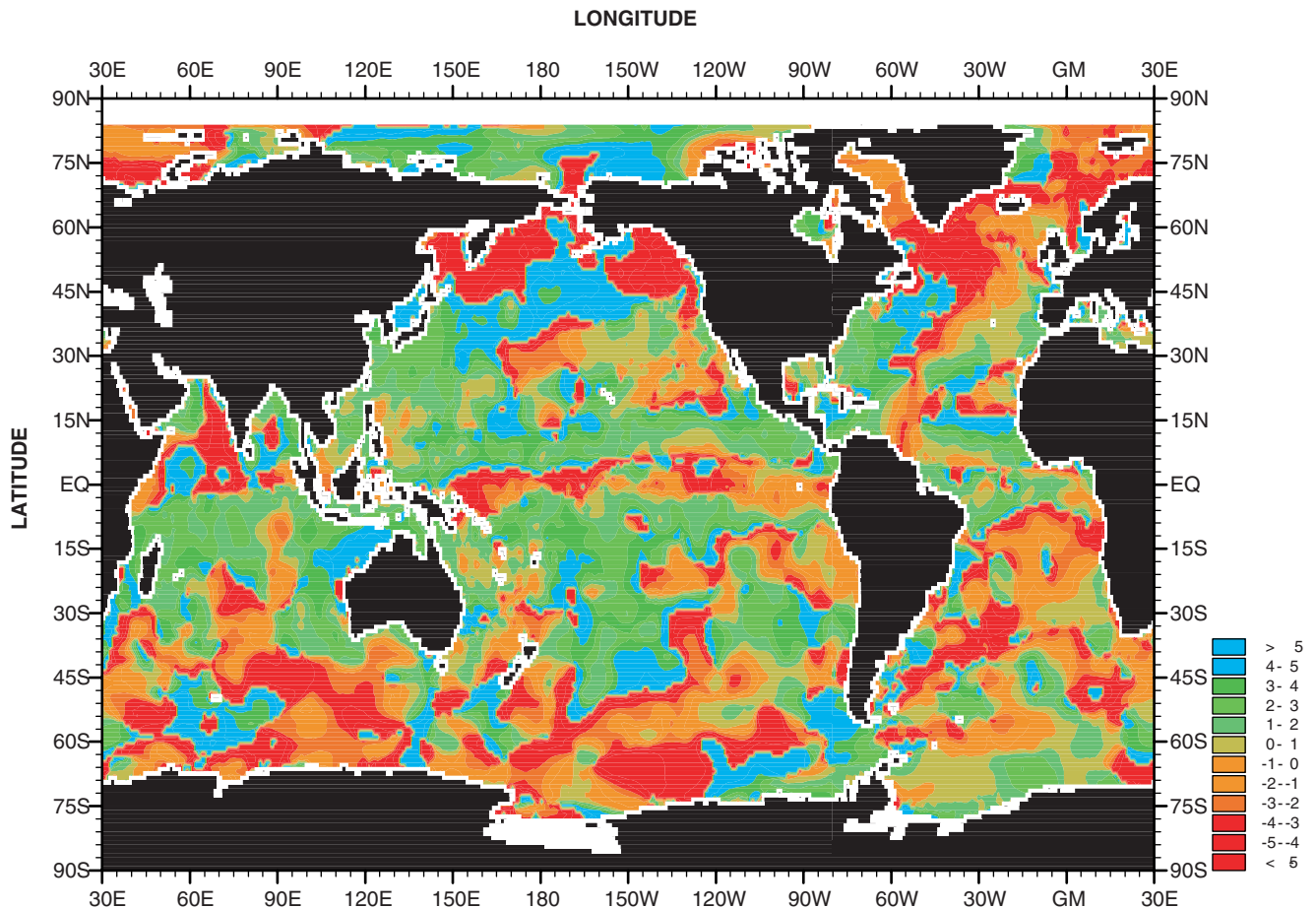
LONGITUDE

Figure 7. Salinity phase lag (months) behind E−P phase.

off the southwest coast of India occurs just to the northeast of this local maximum in SSS variability (Figure 7a). However, on the basis of modeling studies by *Bruce et al.* [1994] and other studies reviewed by *Shenoi et al.* [1999], it appears that remote wind-forcing in the Bay of Bengal that generates Kelvin waves, Rossby waves, and changes in ocean currents plays a dominant role in the annual cycle of this feature. The results of the forcing is that during the Northeast Monsoon, November to February, low salinity water from the Bay of Bengal flows westward into the Arabian Sea between the Indian subcontinent and the island of Sri Lanka [*Shenoi et al.*, 1999], significantly lowering the salinity in the eastern Arabian Sea in the form of relatively warm, fresh anticyclonic eddies. The eddies propagate westward and dissipate which we believe leads to the larger-scale, smooth feature centered at 8°N, 70°E in Figure 3a.

[29] During the Southwest Monsoon, in June to August, high salinity Arabian Seawater flows eastward into the Bay of Bengal, although this flow is interrupted at times by westward flow due to coastal Kelvin waves [*Schott et al.*, 1994].

[30] The influence of the monsoon cycle, while reflected in the amplitude of the first harmonic in the Bay of Bengal, is not as pronounced. The phase of the first harmonic still shows the maximum salinities after the end of the southwest monsoon in the central Bay of Bengal (August to October), possibly reflecting the cumulative effects of the

influx of high salinity water from the Arabian Sea. Nearer the coasts of India, Bangladesh, and Myanmar, the amplitude of the first harmonic of surface salinity is very large, greater than 2.0 in the western and northern Bay of Bengal (Figure 3a). The phase of the first harmonic shows maximum salinities in late April, and slightly earlier in the west (Figure 3b). These coastal amplitudes and phases are associated with river runoff from the many major and minor river systems that empty into the Bay. These include the Godavari to the west, the Ganges/Brahmaputra in the north, and the Irawaddy in the east. All of these river systems have peak outflow in or near August. Minimum outflow is found in late winter/early spring. Differences between maximum and minimum outflows are greater than 40,000 m^3/s for the Brahmaputra, more than 9000 m^3/s for the Irrawaddy, and greater than 10,000 m^3/s for the Godavari [*Balázs et al.*, 2000]. The Ganges and Brahmaputra share a common outflow region into the ocean and have nearly equal annual outflow ranges, but have different annual cycles. The average month of minimum outflow is February for the Bramaputra and April for the Ganges (Table 1). The combined effect of the rivers leads to a month of maximum salinity between the two outflow minima, in March and April, to well over 300 km from the coast. This accounts for the occurrence of maximum salinities found in the near coast areas of the Bay of Bengal in April. The northern winds along the east coast of India during the

southwest monsoon also have the effect of pushing lower salinity coastal waters, mixed with upwelled higher salinity water, offshore into the central Bay of Bengal, dampening the effects of the Arabian Seawater entering the Bay of Bengal at the same time. Most of the northeast Bay of Bengal is characterized by relatively large amplitude in the first harmonic of E−P (Figure 6a).

3.2. Semiannual Cycle of SSS

[31] The amplitude of the second harmonic (Figure 4a) is less than 0.1 over most of the ocean, with areas between 0.1 and 0.3 in the tropics. The amplitude of the second harmonic is greater than 0.3 in the Amazon, Congo, Niger, Mississippi, La Plata, and Ganges/Brahmaputra River outflow regions, as well as the coastal Arctic river outflow/ice cover regions. Except in the Niger outflow the percent of total variance attributed to the second harmonic in these areas is less than 30% (Figure 4b). There are a few other isolated areas where the amplitude of the second harmonic is greater than 0.3 and the percent variance exceeds 30%, most notably Hudson Bay, and near the coast of Antarctica, regions of seasonal ice coverage (and regions with poor data coverage to adequately define the annual cycle or the semiannual cycle). The Indo-Pacific Throughput area also has significant variability associated with the second harmonic. Near the equator south of the Bay of Bengal, the amplitude of the second harmonic accounts for a larger percentage of the total amplitude at the surface than does the amplitude of the first harmonic. This may be associated with the semiannual occurrence of an eastward equatorial jet [*Wyrtki*, 1973].

4. Discussion

[32] With presently available SSS data, a global view of the annual cycle of SSS reveals that the amplitude of the first harmonic of SSS is less than 0.3 for much of the world ocean. Areas with variability greater than 0.3 in the annual cycle in many areas include open-ocean areas in the tropical Pacific under the ITCZ and SPCZ, areas of the North Indian Ocean affected by the monsoons, in the southern Indian Ocean in an area of high E−P variability, in the Indo-Pacific archipelago, in the regions affected by the outflows of major rivers, and in areas of seasonal ice coverage. In conjunction with a global view of the annual cycle of SSS, global data sets of other parameters, such as E−P and river outflows help to understand SSS as part of the global climate system. New data sets becoming available, including salinities from the TAO and PIRATA buoy arrays in the tropical Pacific and Atlantic, high quality thermosalinograph measurements in the tropical Pacific coordinated from ORSTROM, and the Argo profiling float network will greatly improve the quality and reduce the error in future studies of the SSS annual cycle on a global scale.

References

Alory, G., and T. Delcroix, Climatic variability in the vicinity of Wallis, Futuna, and Samoa islands (13°–15°S, 180°–170°W), *Oceanol. Acta*, *22*, 249–263, 1999.

Antonov, J. I., S. Levitus, and T. P. Boyer, Steric sea level variations during 1957–1994: The importance of salinity, *J. Geophys. Res.*, *107*, doi:10.1029/2001JC000964, in press, 2002.

Balázs, M. F., C. J. Vörösmarty, and W. Grabs, Data from *UNH/GRDC Composite Runoff Fields V1.0*, 2000.

Barnier, B., L. Siefridt, and P. Marchesiello, Thermal forcing for a global ocean circulation mode using a three-year climatology of ECMWF analyses, *J. Mar. Syst.*, *6*, 363–380, 1995.

Batteen, M., and M. Huang, Effect of salinity on density in the Leeuwin Current System, *J. Geophys. Res.*, *103*, 24,693–24,721, 1998.

Batteen, M., C. Collins, C. Gunderson, and C. Nelson, The effect of salinity on density in the California Current System, *J. Geophys. Res.*, *100*, 8733–8749, 1995.

Beal, L., A. Ffield, and A. Gordon, Spreading of Red Sea overflow waters in the Indian Ocean, *J. Geophys. Res.*, *105*, 8549–8564, 2000.

Belkin, I., S. Levitus, J. Antonov, and S. Malmberg, "Great Salinity Anomalies" in the North Atlantic, *Prog. Oceanogr.*, *41*, 1–68, 1998.

Bloomfield, P., *Fourier Analysis of Time Series: An Introduction*, 258 pp., John Wiley, New York, 1976.

Bonilla, J., W. Senior, J. Bugden, O. Zafiriou, and R. Jones, Seasonal distribution of nutrients and primary productivity on the eastern continental shelf of Venezuela as influenced by the Orinoco River, *J. Geophys. Res.*, *98*, 2245–2257, 1993.

Borstad, G. A., The influence of meandering Guiana Current and Amazon River discharge on surface salinity near Barbados, *J. Mar. Res.*, *40*, 421–433, 1982.

Boyer, T. P., and S. Levitus, Quality control and processing of historical oceanographic temperature, salinity, and oxygen data, *NOAA Tech. Rep. NESDIS 81*, U.S. Govt. Print. Off., Washington, D. C., 64 pp., 1994.

Boyer, T. P., M. E. Conkright, S. Levitus, C. Stephens, T. O'Brien, D. Johnson, and R. Gelfeld, *World Ocean Database 1998*, vol. 4, *Temporal Distribution of Conductivity-Temperature-Depth Profiles* [CD-ROMs], 163 pp., NOAA Atlas NESDIS 21, U.S. Govt. Print. Off., Washington, D. C., 1998a.

Boyer, T. P., M. E. Conkright, S. Levitus, D. Johnson, J. Antonov, T. O'Brien, C. Stephens, and R. Gelfeld, *World Ocean Database 1998*, vol. 5, *Temporal Distribution of Ocean Station Data (Bottle) Temperature Profiles* [CD-ROMs], 108 pp., NOAA Atlas NESDIS 22, U.S. Govt. Print. Off., Washington, D. C., 1998b.

Boyer, T. P., S. Levitus, J. Antonov, M. Conkright, T. O'Brien, and C. Stephens, *World Ocean Atlas 1998*, vol. 4, *Salinity of the Atlantic Ocean* [CD-ROMs], 166 pp., NOAA Atlas NESDIS 30, U.S. Govt. Print. Off., Washington, D. C., 1998c.

Boyer, T. P., S. Levitus, J. Antonov, M. Conkright, T. O'Brien, and C. Stephens, *World Ocean Atlas 1998*, vol. 5, *Salinity of the Pacific Ocean* [CD-ROMs], 166 pp., NOAA Atlas NESDIS 31, U.S. Govt. Print. Off., Washington, D. C., 1998d.

Boyer, T. P., S. Levitus, J. Antonov, M. Conkright, T. O'Brien, and C. Stephens, *World Ocean Atlas 1998e*, vol. 6, *Salinity of the Indian Ocean* [CD-ROMs], 166 pp., NOAA Atlas NESDIS 32, U.S. Govt. Print. Off., Washington, D. C., 1998e.

Bruce, J. G., D. R. Johnson, and J. C. Kindle, Evidence for eddy formation in the eastern Arabian Sea during the northeast monsoon, *J. Geophys. Res.*, *99*, 7651–7664, 1994.

Cane, M. A., Oceanographic events during El Niño, *Science*, *222*, 1189–1195, 1982.

CLIVAR Scientific Steering Group, CLIVAR Initial Implementation Plan, *WCRP 103*, 313 pp., 1998.

da Silva, A. M., C. Young, and S. Levitus, *Atlas of Surface Marine Data 1994*, vol. 4, *Anomalies of Fresh Water Fluxes* [CD-ROMs], 308 pp., NOAA Atlas NESDIS 9, U.S. Govt. Print. Off., Washington, D. C., 1994.

Delcroix, T., Observed surface oceanic and atmospheric variability in the tropical Pacific at seasonal and ENSO timescales: A tentative overview, *J. Geophys. Res.*, *101*, 18,611–18,633, 1998.

Delcroix, T., C. Henin, V. Porte, and P. Arkin, Precipitation and sea-surface salinity in the tropical Pacific Ocean, *Deep-Sea Res.*, *43*, 1123–1141, 1996.

Dessier, A., and J. Donguy, The sea surface salinity in the tropical Atlantic between 10°S and 30°N—seasonal and interannual variations (1979–1989), *Deep-Sea Res.*, *41*, 81–100, 1994.

Dickson, R. R., J. Meincke, S. Malmberg, and A. Lee, The "Great Salinity Anomaly" in the North Atlantic, 1968–1982, *Prog. Oceanogr.*, *20*, 103–151, 1988.

Donguy, J. R., Surface and subsurface salinity in the tropical Pacific Ocean. Relations with climate, *Prog. Oceanogr.*, 34, 45–78, 1994.

Donguy, J. R., and G. Meyers, Seasonal variations of sea-surface salinity and temperature in the tropical Indian Ocean, *Deep-Sea Res.*, 43, 117–138, 1996a.

Donguy, J. R., and G. Meyers, Mean annual variation of transport of major currents in the tropical Pacific Ocean, *Deep-Sea Res.*, 43, 1105–1122, 1996b.

Forsbergh, E. D., On the climatology, oceanography, and fisheries of the Panama Bight, *Bull-Inter.-Am. Trop. Tuna Comm.*, 14, 49–385, 1969.

Froelich, P. N., D. Atwood, and G. Giese, Influence of Amazon River discharge on surface salinity and dissolved silicate concentrations in the Caribbean Sea, *Deep-Sea Res.*, 25, 735–744, 1978.

Henin, C., and J. Grelet, A merchant ship thermo-salinograph network in the Pacific Ocean, *Deep-Sea Res.*, 43, 1833–1855, 1996.

Henin, C., Y. du Penhoat, and M. Ioualalen, Observations of sea surface salinity in the western Pacific fresh pool: Large-scale changes in 1992–1995, *J. Geophys. Res.*, 103, 7523–7536, 1998.

Hires, R., and R. Montgomery, Navifacial temperature and salinity along the track from Samoa to Hawaii, 1957–1965, *J. Mar. Res.*, 30, 177–200, 1972.

Hur, H. B., G. A. Jacobs, and W. J. Teague, Monthly variations of water masses in the Yellow and East China Seas, November 6, 1998, *J. Oceanogr.*, 55, 171–184, 1999.

Khatiwala, S. P., R. G. Fairbanks, and R. Houghton, Freshwater sources to the coastal ocean off northeastern North America: Evidence from $H_2^{18}O$/ $H_2^{16}O$, *J. Geophys. Res.*, 104, 18,241–18,255, 1999.

Kumar, S., and T. Prasad, Formation and spreading of Arabian Sea high-salinity water mass, *J. Geophys. Res.*, 104, 1455–1464, 1999.

Lentz, S. J., Seasonal variations in the horizontal structure of the Amazon Plume inferred from historical hydrographic data, *J. Geophys. Res.*, 100, 2391–2400, 1995.

Levitus, S., *Climatological Atlas of the World Ocean, NOAA Prof. Pap. 13*, 173 pp., with microfiche attachments, U.S. Govt. Print. Off., Washington, D. C., 1982.

Levitus, S., Annual cycle of salinity and salt storage in the world ocean, *J. Phys. Oceanogr.*, 16, 322–343, 1986.

Levitus, S., Interpentadal variability of temperature and salinity at intermediate depths of the North Atlantic Ocean, 1970–74 versus 1955–59, *J. Geophys. Res.*, 94, 6091–6131, 1989.

Levitus, S., M. E. Conkright, T. P. Boyer, T. O'Brien, J. Antonov C. Stephens, L. Stathoplos, D. Johnson, and R. Gelfeld, *World Ocean Database 1998*, vol. 1, *Introduction* [CD-ROMs], 346 pp., NOAA Atlas NESDIS 18, U.S. Govt. Print. Off., Washington, D. C., 1998.

Lukas, R., Freshening of the upper thermocline in the North pacific subtropical gyre associated with decadal changes of rainfall, *Geophys. Res. Lett.*, 28, 3485–3488, 2001.

Lukas, R., and E. Lindstrom, The mixed layer of the western equatorial Pacific Ocean, *J. Geophys. Res.*, 96, suppl., 3343–3357, 1991.

Lynn, R., and J. Reid, Characteristics and circulation of deep and abyssal circulation, *Deep Sea Res.*, 15, 577–598, 1968.

Maes, C., Estimating the influence of salinity on sea level anomaly in the ocean, *Geophys. Res. Lett.*, 25, 3551–3554, 1998.

Miyama, T., T. Awaji, K. Akitomo, and N. Imasato, A Lagrangian approach to the seasonal variation of salinity in the mixed layer of the Indonesian Seas, *J. Geophys. Res.*, 101, 12,265–12,285, 1996.

Müller-Karger, C. McClain, T. Fisher, W. Esaias, and R. Varela, Pigment distribution in the Caribbean Sea: Observations from space, *Prog. Oceanogr.*, 23, 23–64, 1989.

Pailler, K., B. Bourlès, and Y. Gouriou, The Barrier Layer in the western Tropical Atlantic Ocean, *Geophys. Res. Lett.*, 26, 2069–2072, 1999.

Parkinson, C., D. Cavalieri, P. Gloersen, H. Zwally, and J. Comiso, Arctic sea ice extents, areas, and trends, 1978–1996, *J. Geophys. Res.*, 20,837–20,856, 1999.

Reverdin, G., D. Cayan, H. Dooley, D. Ellett, S. Levitus, Y. Du Penhoat, and A. Dessier, Surface salinity of the North Atlantic: Can we reconstruct its fluctuations over the last one hundred years?, *Prog. Oceanogr.*, 33, 303–346, 1994.

Schott, F., J. Reppin, J. Fischer, and D. Quadfasel, Currents and transports of the Monsoon Current south of Sri Lanka, *J. Geophys. Res.*, 99, 25,127–25,141, 1994.

Shenoi, S., D. Shankar, and S. R. Shetye, On the sea surface temperature high in the Lakshadweep Sea before onset of the southwest monsoon, *J. Geophys. Res.*, 104, 15,703–15,712, 1999.

Smed, J., Annual and seasonal variations in the salinity of the North Atlantic surface water, in *Rapports et Proces-Verbaux des Reunions*, vol. CXII, *Hydrography*, pp. 79–94, And. Fred. Host and Fils, Copenhagen, Denmark, 1943.

Taylor, A. H., Seasonal and year-to-year variations in surface salinity at the nine North Atlantic Ocean Weather Stations, *Oceanol. Acta*, 3, 330–421, 1980.

Taylor, A. H., Fluctuations in the surface temperature and surface salinity of the north-east Atlantic at frequencies of one cycle per year and below, *J. Climatol.*, 3, 253–269, 1983.

Taylor, J. R., *An Introduction to Error Analysis*, 327 pp., Univ. Sci. Books, Sausalito, Calif., 1997.

Vialard, J., and P. Delecluse, An OGCM study for the TOGA Decade, part II, Barrier-layer formation and variability, *J. Phys. Oceanogr.*, 28, 1089–1106, 1998.

Waliser, D. E., and C. Gautier, A satellite-derived climatology of the ITCZ, *J. Clim.*, 6, 2162–2174, 1993.

Wyrtki, K., A equatorial jet in the Indian Ocean, *Science*, 181, 262–264, 1973.

Yamagata, T., K. Mizuno, and Y. Masumoto, Seasonal variations in the equatorial Indian Ocean and their impact on the Lombok throughflow, *J. Geophys. Res.*, 101, 12,465–12,471, 1996.

――――――――――――――

T. P. Boyer and S. Levitus, Ocean Climate Laboratory/National Oceanographic Data Center, Silver Spring, MD, USA. (boyer@nodc.noaa. gov)